Application of a new distributed hydrological model based on soil–gravel structure in the Niyang River Basin, Qinghai–Tibet Plateau

Pengxiang Wang[1,2,3], Zuhao Zhou[1*], Jiajia Liu[1], Chongyu Xu[3,7], Kang Wang[3], Yangli Liu[4], Jia Li[5], Yuqing Li[6], Yangwen Jia[1], Hao Wang[1]

[1]State Key Laboratory of Simulation and Regulation of Water Cycle in River Basin, China Institute of Water Resources and Hydropower Research, Beijing 100038, China
[2]China Three Gorges Corporation, Beijing 100038, China
[3]State Key Laboratory of Water Resources and Hydropower Engineering Science, Wuhan University, Wuhan 430072, China
[4]China Power Construction Group Guiyang Engineering Corporation Limited, Guiyang 550081, China
[5]Bureau of South to North Water Transfer of Planning, Designing and Management, Ministry of Water Resources, Beijing 100038, China
[6]Department of Water Resources and Civil Engineering, Tibet Agriculture and Animal Husbandry College, Nyingchi 860000, China
[7]Department of Geosciences, University of Oslo, Oslo, Norway

Correspondence to: Zuhao Zhou (zhzh@iwhr.com)

Abstract: Runoff formation and hydrologic regulation mechanisms in mountainous cold regions are the basis for investigating the response patterns of hydrological processes under climate change. The Qinghai-Tibet Plateau (QTP) has a thin soil layer on top of a thick soil-gravel mixture (SGM) layer. This unique geological structure, combined with the snow and frozen soil in this area, significantly affect water circulation in the entire region. To investigate the influence of the underlying surface structure on the water-heat transport and water circulation process in the QTP, we performed a comprehensive study combining water and heat transfer field experiments and developed a Water and Energy transfer Processes model in the QTP (WEP-QTP), based on the original Water and Energy transfer Processes model in Cold Regions (WEP-COR). The Niyang River Basin located on the QTP was selected as the study area to evaluate the consistency between theoretical hypothesis, observation, and modeling results. The model divides the uniform soil profile into a dualistic soil and gravel structure. When no phase change occurs in the ground, two infiltration models based on the dualistic soil-gravel structure were developed using the Richards equation in a non-heavy rain scenario and the multi-layer Green-Ampt model in a heavy rain scenario. During the freeze–thaw period, a water-heat coupling model based on the continuum of the snow-soil-gravel layer was constructed. The addition of the SGM layer corrected the original model's overestimation of the moisture content below the surface soil and reduced the moisture content relative error (RE) from 33.74 to -12.11%. The addition of the snow layer not only reduced the temperature fluctuation of the surface soil, but also, with the help of the SGM layers, revised the original model overestimation of the freeze-thaw speed. The temperature RMSE was reduced from 1.16 °C to 0.86 °C. In the fully thawed period, the dualistic soil-gravel structure improved the regulation effect of groundwater on flow, stabilizing the flow process. The maximum RE at the flow peak and valley decreased by 88.2 and 21.3%, respectively. In the freeze-thaw period, by considering the effect of the snow-soil-gravel layer continuum, the freezing and thawing process of

WEP-QTP lagged that of WEP-COR by approximately one month. The groundwater simulated by WEP-QTP had more time to recharge the river, which better showed the observed "tailing" process after September. The flow simulated by the WEP-QTP model was more accurate and closer to the actual measurements, with Nash > 0.75 and |RE| < 10 %. The improved model reflects the effects of the unique QTP environment on water-heat transport and water cycle process and can be used for hydrological simulation in the QTP.

1 Introduction

The Qinghai-Tibet Plateau (QTP), known as the “Asian Water Tower,” is a major cold mountainous area with low latitude and high altitude. This region has unique geology and landform, is sensitive to climate change (Liu et al., 2019), and is vital for the water resources security of China and Southeast Asia (Yu et al., 2012). The extensive glaciers, snow cover, permanently and seasonally frozen soil in the area have major impacts on the water cycle (Li et al., 2016; Ding et al., 2020). Unraveling the runoff formation and hydrological regulation mechanisms in this region is the basis for studying the response patterns of hydrological processes under climate change conditions.

In both the permafrost and permafrost-free areas, the ground undergoes seasonal freezing and thawing, which has received a lot of attention regarding hydrological research because of the great variety of biological and physical processes occurring at the surface and subsurface (Chen et al., 2014; Kurylyk et al., 2014). During soil freezing, ice in the seasonal thaw layer blocks most of the pores in the soil, hinders infiltration, and affects water movement in the soil (Cheng and Jin, 2013). As for the hydrological cycle, the frozen soil layer prevents rainfall and snowmelt infiltration, forcing surface runoff down the slope, which may lead to severe flash floods. In addition, it affects the quantity of groundwater recharge supplemented by infiltration and the distribution ratio of surface runoff between rivers and lakes (Ireson et al., 2013; Larsbo et al., 2019). The simulation accuracy of the water and heat transport in the seasonal thaw layer directly affects the evaluation of water resources in this area and the analysis of the runoff evolution. However, soil water and heat transfer are relatively complex and influenced by several factors (Watanabe and Kugisaki, 2017) such as soil structure (Dai et al., 2019; Franzluebbers, 2002) and heat conduction under snow cover (Lundberg et al., 2016).

During the continuous QTP uplift, a series of ascending areas (denuded areas) and descending areas (deposited areas) have been formed. Quaternary deposits are generally thinner in denuded areas and thicker in deposited areas (valleys, plain). As a result of the surface uplift and collision of the Indian plate with the Eurasian plate, there are many gravel and rock fragments, which are soil-gravel mixtures (SGM), in the QTP Quaternary sediments. SGM has hydraulic and thermodynamic properties distinct from that of soil, which are affected by the sand and gravel content (Zhang et al., 2011). When this content is low, the gravel changes the SGM structure and increases the distance of water movement; the saturated hydraulic conductivity of SGM decreases as the gravel content increases (Childs and Flint, 1990; Mehuys et al., 1975). When the sand and gravel content exceeds a certain level, connected macropores are formed in the SGM, and the saturated hydraulic conductivity increases along with the content (Beibei et al., 2009). In the heat transfer process, the greater thermal conductivity and heat

capacity of gravel compared with those of dry soil affect the heat transfer(Yi et al., 2013). In addition, under strong freeze-thaw conditions in the cold plateau region, the humus accumulation of herbaceous plants is slow, while the decomposition of minerals is weak, resulting in slow soil development on the surface of Quaternary deposits and a thin soil layer above the SGM (Deng et al., 2019; Yang et al., 2009; Chen et al., 2015; Sun, 1996).

The existing hydrological models in cold regions, such as the SHAWDHM model (Zhang et al., 2013), GEOtop model (Rigon et al., 2006), Cold Regions Hydrological Model (CRHM) (Pomeroy et al., 2007), and Variable Infiltration Capacity (VIC) model (Cherkauer and Lettenmaier, 2003), consider the processes of water and heat transport in the soil in cold regions and can simulate the water cycle processes in generally cold regions to a certain extent. However, these models define the simulated object of water-heat coupled transport process as a one-dimensional homogeneous medium, while overlooking the upper and lower layered structure of the QTP. By calibrating the parameters, the difference in water and heat transfer between SGM and soil can be hidden to some extent, and the simulation effect can be improved. However, there remain some errors in the simulation, and it is difficult to objectively reflect the influence of the upper and lower geological structures on water-heat transport and the hydrological cycle.

It is particularly important to consider the influence of the unique underlying surface of the QTP on the water-heat transport and water circulation, especially in the context of global climate change and frozen soil degradation. The objectives of the present study were to: (1) develop infiltration models based on the dualistic soil–gravel structure under the fully thawed conditions, (2) develop a modeling framework representing coupled heat and water transfers in the ground based on snow–soil–gravel layer continuum through field water and heat monitoring experiments during the freeze–thaw period (the soil/SGM layer temperature of the calculation unit was lower than 0 ℃), and (3) investigate the effect of the dualistic soil–gravel structure on the hydrological cycle by building the distributed water cycle model (WEP-QTP) for the Niyang River Basin, a tributary of the Yarlung Zangbo River in the QTP.

2 Materials and methods

2.1 Study sites and data

2.1.1 Study area

The Niyang River is located on the left bank of the lower reaches of the Yarlung Zangbo River, between 29°28'–30°38' N and 92°10'–94°35' E in the Linzhi area of southeastern Tibet. It originates from Cuomoliang Mountain on the west side of the Mila Mountain in the Tibet Autonomous Region of China at an altitude of approximately 5,000 m above sea level (a.s.l.). The Niyang River flows through Gongbujiangda County and Bayi Town from west to east and finally flows into the Yarlung Zangbo River in the Bayi District of Nyingchi City, with a drop of 2,080 m and an average slope drop of 0.73 %. The basin is approximately 230 km long from east to west, and 110 km wide from north to south. The area of the watershed is 17,535 km^2, ranking fourth among the five tributaries of the Yarlung Zangbo River, and its runoff is second only to that of

Palungzangbu. The Niyang River Basin is located at the intersection of Tibet's east–west and north–south mountain ranges. The basin sediments consist of greywacke and litharenite with low-moderate maturities of textures and minerals (Huyan et al., 2022). The terrain in the watershed is complex, with staggered large and small mountains and large elevation fluctuations. The elevation of the river valley is generally 3,000–4,000 m a.s.l. The elevation of most mountain peaks on both sides of the valley is approximately 5,000 m a.s.l, reaching up to 6,870 m a.s.l. The Niyang River Basin belongs to the plateau temperate monsoon climate zone. The multi-year average precipitation is affected by the Indian Ocean tropical ocean monsoon. Under the effect of the Indian low pressure, the southwest monsoon pushes a large amount of warm and humid air from the Bay of Bengal along the Yarlung Zangbo River Valley to the Niyang River Basin, causing precipitation in the basin with heavy rainfall and large vertical changes. The average elevation of the basin is 4688.6 m a.s.l, the average annual precipitation is 1,416 mm, and the average annual temperature is approximately 8 °C. Obvious temperature changes occur from east to west with elevation. The frozen soil in the study area is mainly seasonal. Permafrost accounts for approximately 24% of the basin area, mainly distributed in the upper reaches of the basin and the high-altitude areas on both sides of the mainstream.

In the present study, a water-heat coupling process monitoring experiment was carried out during the freeze–thaw period on the mountainside of the Sejila Mountain in the lower reaches of the Niyang River Basin. The longitude and latitude of the study site are 94°21′45″ E and 29°27′12″ N, respectively, and the altitude is 4,607 m a.s.l. The annual average temperature of the experimental site is 5.28 ℃, which is a seasonally frozen soil area. The experimental period was 2016–2017, while the freeze–thaw period was from November 2016 to March 2017. The station distribution of the watershed and the location of the experimental points are shown in Figure 1. Before the field experiment, nuclear magnetic resonance was used to calibrate the water and heat transport monitoring instruments under seasonal freezing and thawing soil conditions on the plateau. A working area with a length of 1.0 m, a width of 1.0 m, and a depth of 2.0 m was excavated at the experimental site. A time-domain reflectometry sensor was used to monitor the contents of the liquid water, a PT100 sensor was used to measure the temperature, and a TensionMark sensor was used to measure the soil water potential, all of which were installed every 10 cm vertically in the experimental pit to a depth of 1.6 m. Following installation, the pit was backfilled with undisturbed soil and the data were collected automatically.

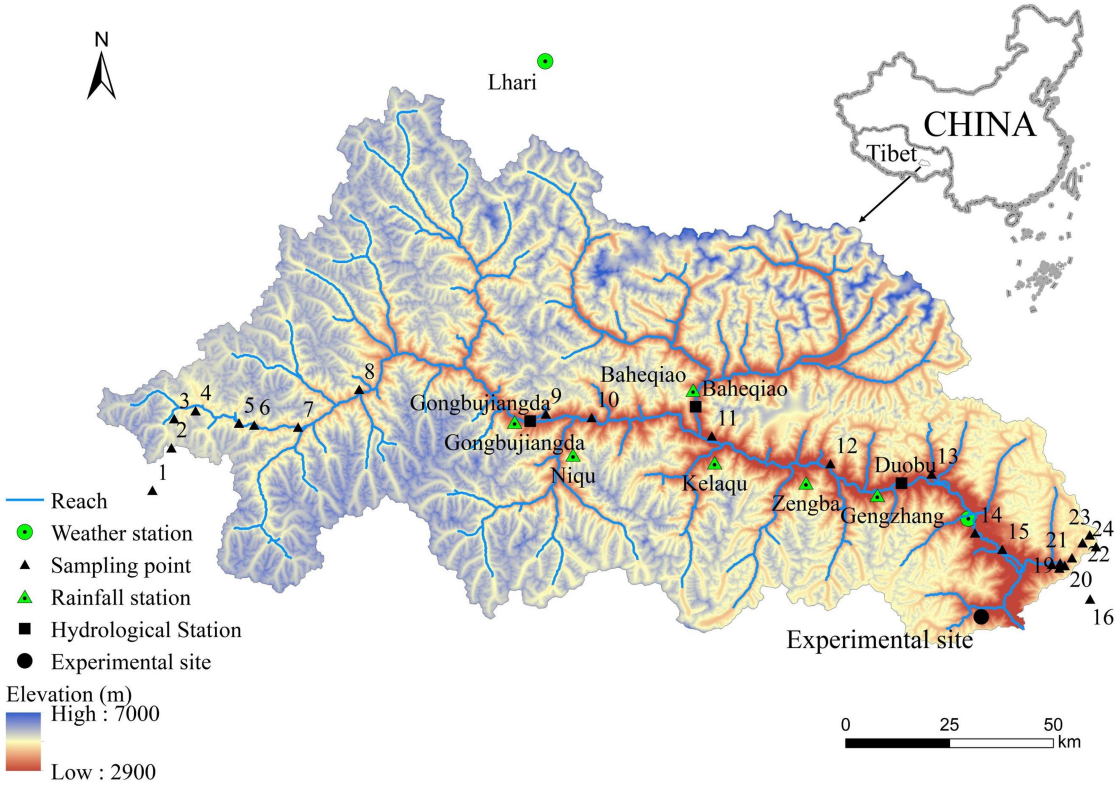

Figure 1: Basic situation and station distribution of the Niyang River Basin

2.1.2 Data description

The data required for this study were mainly divided into two categories: the first were data required for model construction (mainly including meteorology, geology and landform, terrain, soil type, land-use type, vegetation index, and glacier data), while the second were data used to verify the model results (including historical and experimental monitoring data).

Meteorological data: temperature, relative humidity, sunshine hours, and wind speed data were collected by the Nyingchi Meteorological Station in the basin and the Jiali Meteorological Station outside the basin, from 1961–2018. The data were obtained from the China Meteorological Data Network (http://data.cma.cn). In addition to the two meteorological stations in Nyingchi and Jiali, the rainfall data sources also included six rainfall stations (2013–2015) including Gongbujiangda, Gengzhang, Baheqiao, Niqu, Kelaqu, and Zengba in the watershed and the contour map of annual precipitation in the Tibet Water Resources Bulletin (2012–2017). The temperature, precipitation, relative humidity, sunshine duration, and wind speed in the basin were interpolated from the meteorological station data by the reversed distance squared method. Temperature and precipitation were additionally corrected for elevation. The temperature correction factor was -6 °C/km. As for the precipitation data, the precipitation-elevation relationship was determined according to the contour map of annual precipitation in the Tibet Water Resources Bulletin and the precipitation station data. Subsequently, the daily precipitation

data were obtained in the basin through elevation interpolation (Wang et al., 2017) of the precipitation data from six rainfall stations and two meteorological stations to avoid precipitation errors at high altitudes caused by altitude limitations of precipitation stations.

Geology and landform: Due to the combined effects of plate tectonics, weathering, and erosion, a unique geological structure was formed in the QTP with a thin soil layer on the top and a thick SGM layer on the bottom (Fig. 2). According to the geological characteristics of the QTP, we selected 24 sampling points at different altitudes from the source to the estuary of the Niyang River basin for field investigation on soil texture (Fig. 1). Among them, points 1–16 were along the river, while 17–24 were from the foot of the mountain to the peak. The soil thicknesses and compositions at the 24 sampling points were measured and analyzed. The soil layer of the Niyang River Basin is mainly sandy loam, with average sand, silt, and clay contents of 55.89, 31.2, and 12.91%, respectively. The SGM layer is mainly round gravel containing pebbles; the gravel content was approximately 50–65%, the clay content was 5–10%, and the pores are filled with medium and fine-grained sand. The thickness of the soil layer gradually decreases from the foot to the peak of the mountain, and is approximately 40 cm on the hillside with higher altitude and increases to more than 100 cm in the valley.

Figure 2: Soil and gravel structure of the Niyang River Basin (pictures taken near the experimental site in Figure 1)

Terrain data: The elevation data (Digital Elevation Model, DEM) used in this study were obtained from the SRTM90 (Shuttle Radar Topography Mission), jointly measured by the National Aeronautics and Space Administration (NASA) and the National Imagery and Mapping Agency (NIMA) with an accuracy of 90 m.

Soil date: Soil type data were obtained from the second national soil census and “Chinese Soil Records”. Land-use data were obtained from the Resource Environment Science and Database Center, Institute of Geographic Sciences and Natural Resources Research, Chinese Academy of Sciences (http://www.resdc.cn), and the data resolution was 30 m.

Vegetation index: Moderate-resolution Imaging Spectroradiometer (MODIS) data (https://ladsweb.modaps.eosdis.nasa.gov/search/) from 2000–2017 were selected as the data source. Among them, the leaf area index accuracy was 500 m and the normalized difference vegetation index accuracy was 250 m; these were mainly used to calculate evaporation and vegetation interception processes, respectively.

Glacier data: The glacier data included China's second glacier inventory data set (1:100,000) and Landsat TM/ETM+/OLI remote sensing images. The second glacier inventory data were obtained from the China Cold and Arid Regions Science Data Center (http://westdc.westgis.ac.cn/). Landsat data were obtained from the data sharing platform of the United States Geological Survey (USGS) (http://glovis.usgs.gov/). ENVI software was used to extract glaciers, and the boundaries of the glaciers were finally determined with reference to Google Earth imagery. The glaciers in the basin were classified according to China's second glacier cataloging rules and the glacier area was calculated. The volume of the glacier was calculated by the area-volume empirical formula (Grinsted, 2013; Radić and Hock, 2010).

The distribution of the main hydrologically-relevant features of the basin used in the model construction is shown in Appendix A.

Model verification data included historical data and experimental monitoring data. Historical data included daily measured flow data from the Gongbujiangda Hydrological Station (2013–2016, 2018), the Baheqiao Hydrological Station (2013–2014), and the Duobu station (2013–2018). The experimental monitoring data included the soil temperature and volumetric water content of the experimental site from 2016–2017.

2.2 Model improvement

Based on the Water and Energy transfer Processes in Cold Regions (WEP-COR) model (Li et al., 2019), this study developed the improved Water and Energy transfer Processes in the QTP (WEP-QTP) model. The WEP-COR model is a distributed hydrological model. To consider the impact of the topography and land cover on the water cycle in large basins, the calculation unit of the WEP-COR model is contour bands (i.e., bands at different elevation intervals) inside small sub-basins. Each unit is classified into five classes: water body, soil–vegetation, irrigated farmland, non-irrigated farmland, and impervious area (The water body class includes rivers, lakes and glaciers. The soil – vegetation class includes bare land, grassland and woodland. Impervious area consists of urban buildings and impervious surfaces). The calculation result of the water and heat flux in each type was weighted by area to obtain the water and heat flux of the contour band. An introduction to the WEP-COR model structure and simulation method is provided in Appendix B.

In contrast to the general cold areas where the WEP-COR model is applied, the widespread dualistic soil–gravel structure in the QTP has a great impact on the water cycle processes in the basin. The seasonal thaw layers above the impervious boundary, including the aquifer and vadose zone, were investigated (in permafrost regions, the impervious boundary is the permafrost layer). This part contains both soil and SGM layers with a strong freeze-thaw effect, closely interacts with the surface hydrological process, and is the key link affecting the hydrological cycle in this area. Based on the geological characteristics of the QTP, the water and heat simulation methods for the fully thawed and freeze-thaw periods of soil-vegetation, irrigated farmland, and non-irrigated farmland were improved as follows.

Under the fully thawed conditions, the calculation object of water movement was defined as the dualistic soil–gravel structure (Fig. 3a). The upper layer was soil, whose thickness is determined by the location of the calculation unit, and which gradually decreased gradually from the foot to the peak of the mountain (Fig. 3b). The lower layer is the SGM layer. During

the freeze–thaw period, in addition to considering the impact of gravel on water–heat transfer, the contribution of snow to thermal insulation and its higher reflectivity to shortwave solar radiation were also considered. A snow layer was added on top of the dualistic soil–gravel structure. The water–heat coupling simulation object was defined as the snow–soil–gravel layer continuum (Fig. 3c).

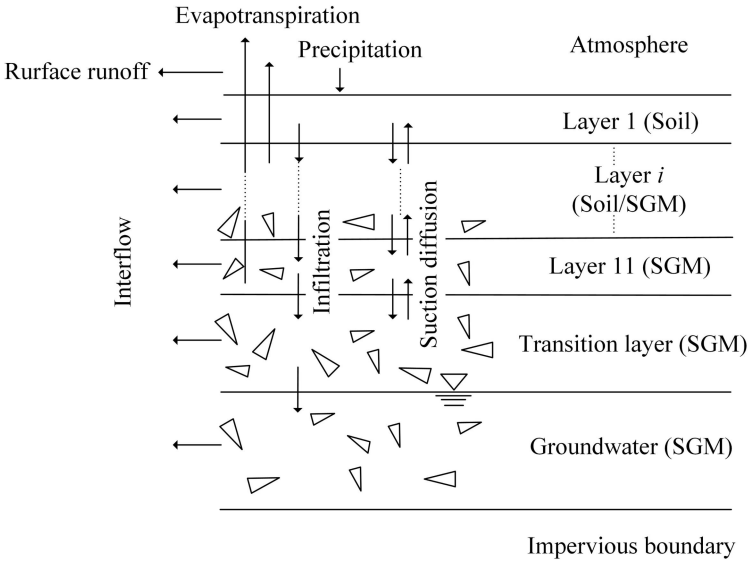

(a)

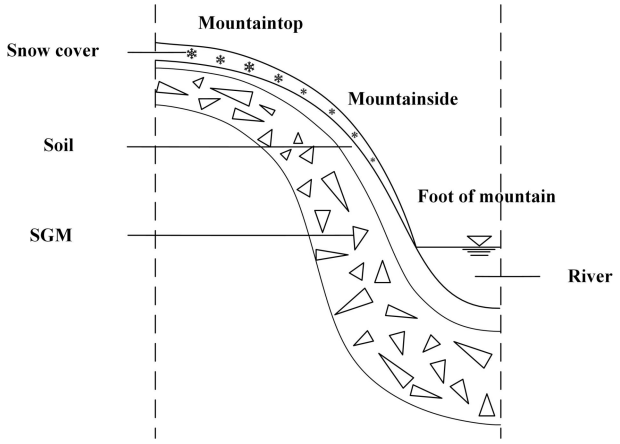

(b)

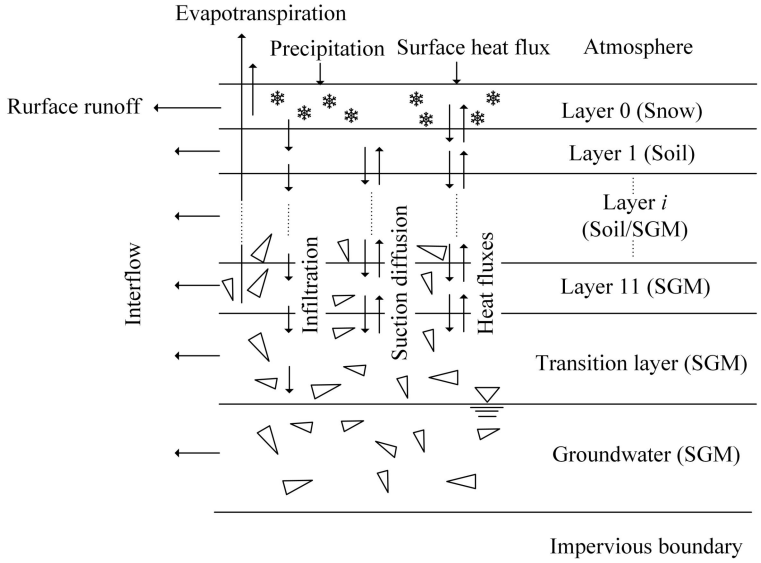

(c)

Figure 3: Layered calculation structure of the dualistic "soil–gravel" structure (a), snow–soil–gravel layered structure (b) and the "snow–soil–gravel layer" continuum (c)

As the surface soil is more sensitive to changes in atmospheric temperature, the thicknesses of the first and second layers were set to 10 cm each, while the third through the eleventh layers were divided evenly, each with a thickness of 20 cm. The depth from the surface to the impermeable layer was an adjustable parameter in the model that can be adjusted based on the actual basin conditions. Considering the active range of seasonal frozen soil, the depth of the water–heat numerical simulation in the model was set 2 m. When the depth of impermeable layer was greater than 2 m, the excess comprised the transition layer. The lower boundary at the bottom was the impermeable layer, assuming that it maintains a constant temperature (seasonal frozen soil regions > 0 °C, permafrost regions < 0 °C). In regions with seasonally frozen soil, the model considered the entire freezing and bidirectional thawing processes of the soil. For the permafrost regions, the surface layer freezing and thawing processes were considered, while the lower permafrost layer was used as the lower boundary condition.

2.2.1 Fully thawed period

In the non-heavy rain infiltration scenario, the basic equations describing water movement were the same as the WEP-COR model. However, in the unsaturated state, since gravel can neither conduct nor store water, the gravel, which accounts for 50–65% of the SGM layer, hinders the movement of water and affects the water retention curves (Cousin et al., 2003). Therefore, the revised formula for water retention properties of the soil–gravel mixture was used to describe the lower gravel layer water retention curves (Wang et al., 2013):

$$\frac{\theta_l-\theta_r}{\theta_s-\theta_r} = A_m h^{-\lambda}\left(1 - B_m \omega_{gravel}\right) \quad (1)$$

where A_m and B_m are empirical parameters, h is the matric suction (cm), λ is the pore-size distribution parameter ($\lambda < 1$), and ω_{gravel} is the volume ratio of the gravel in the SGM layer.

In the heavy rain infiltration scenario, the multi-layer Green–Ampt equation (Jia and Tamai, 1998) was used to calculate the infiltration process when the infiltration front (INF) was in the soil layer, which is the same as in WEP-COR (Equation B4 to B11 in Appendix B). When the INF moves to the interface of the soil and SGM (Layer *itf*), the front movement slows down because the water suction of the SGM layer is less than that of the soil (Mao and Shang, 2010). Until the water has the same potential energy in the soil and the SGM, the INF breaks through the critical surface, and then the infiltration rate stabilizes (Fig. 4). Therefore, a new infiltration model was proposed by improving the method of infiltration rate in the multi-layer Green–Ampt equation (Equation B4 in Appendix B). The stable infiltration rate after INF breaking through Layer *itf* was calculated as follows:

$$f_{gravel} = k_{soil}\left(1 + \frac{A_{itf}}{B_{itf}+F_{itf}}\right) \quad (2)$$

where f_{gravel} is the stable infiltration rate after breaking through Layer *itf*; k_{soil} is the saturated hydraulic conductivity of the soil layer (mm/h); A_{itf} is the total water capacity of the soil above the interface (mm); B_{itf} is the error caused by the different soil moisture content of the soil above the interface (mm); F_{itf} is the cumulative infiltration when the front breaks through Layer *itf* (mm).

The gravel increases the porosity in the SGM layers, and the pores connect to form a fast channel for transporting water during heavy rains. After the INF breaks through the interface, the infiltration water preferentially recharges the groundwater through the macropores. The accumulated infiltration quantity is as follows:

$$F = F_{itf} + Q_{gd} \quad (3)$$

where Q_{gd} is the quantity of groundwater recharge by infiltration, $Q_{gd} = f_{gravel}(t - t_{itf})$, and t_{itf} is the time when the INF breaks through the interface.

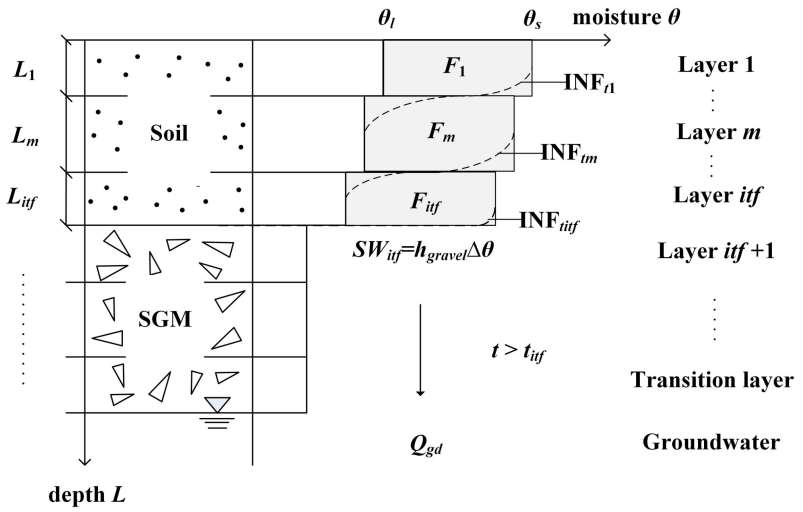

Figure 4: Cumulative infiltration process of the WEP-QTP model

Under the fully thawed conditions, all the water was in a liquid state, and the heat conduction had a minor effect on the water migration process. Therefore, for simulation efficiency, only the moisture simulation was performed during this period.

2.2.2 Freeze–thaw period

During the freeze-thaw period, the water–heat coupling simulation object was defined as the snow–soil–gravel layer continuum (Fig. 3b). A snow layer was added on top of the dualistic soil–gravel structure, the thickness of which was determined by the snow water equivalent and snow density. In the QTP, differences in temperature and precipitation caused by altitude differences cause the calculation units (the contour bands) at higher altitudes to accumulate more snow and less melting. Conversely, calculation units with lower elevations accumulate less snow and more melting. In this model, we established a thickness threshold. When the snow thickness difference between two calculation units exceeded this threshold, snow meltdown occurred. The snow in the higher-altitude calculation unit slides into the next unit until the two units have the same snow thickness. The daily variation of snow water equivalent was calculated as follows:

$$S = S_p - S_d - S_m \quad (4)$$

where S is the daily variation of snow water equivalent (mm/d); S_p is the snow water equivalent from precipitation (mm/d), S_p is equal to the daily precipitation when the average atmospheric temperature of the day was less than 2 °C, otherwise S_p = 0; S_d is the snow water equivalent variation due to snow sliding down (mm/d), when the difference in snow thickness between two adjacent contour bands exceeds this threshold, an avalanche occurs between those contour bands. The snow in the higher-altitude contour band slides into the lower band until the two bands equalize in snow thickness.; S_m is the quantity of snow melting equivalent (mm/d) calculated using the degree-day factor method (Hock, 1999) as follows:

$$S_m = d_f(T_a - T_S) \quad (5)$$

where d_f is the degree-day factor (mm/[°C·day]); T_a is atmospheric temperature (°C), T_S is the critical temperature of snow melting (°C), assuming snow melt starts when T_a is > T_S. S_m was treated as precipitation in the model.

The simulation method of water transport under the snow layer was the same as that in fully thawed period. But the saturated hydraulic conductivity (K_s) of the soil or SGM layer was corrected by temperature and can be calculated as follows (Chen et al., 2008; Jansson, 2004):

$$K_s = \begin{cases} K & T > 0 \\ K(0.54 + 0.023T) & T_f \le T \le 0, \\ K_0 & T < T_f \end{cases} \quad (6)$$

where K is the initial saturated hydraulic conductivity (cm/s) and K_0 is the minimum hydraulic conductivity (cm/s) under freezing conditions. Considering the difference in the hydrodynamic properties of the soil and SGM layer, the K_0 value for soil was 0 cm/s. For the SGM layer, due to the larger pores, K_0 has a value > 0 cm/s; T is the temperature of the soil or SGM layer (°C), while T_f is the critical temperature (°C) corresponding to the minimum hydraulic conductivity.

For the heat transfer process, assuming that the upper boundary of the system is the atmosphere, which controls the input and output of the system energy. In the presence of snow on the surface, the atmosphere first exchanges energy with the snow layer, and then the snow layer exchanges energy with the soil. Conversely, in the absence of snow, the atmosphere directly exchanges energy with the soil, and the energy fluxes can be calculated based on the climate forcing. The lower boundary at the bottom is the impermeable layer, assuming that it maintains a constant temperature (seasonal frozen soil regions > 0 °C, permafrost regions < 0 °C). The heat transferred to the underlying surface is calculated using the following equation (Hu et al., 2001; Jia et al., 2001):

$$\mathrm{G} = C_{Vu} d_u (T_a - T_u) \quad (7)$$

where, C_{Vu} is the volumetric heat capacity of the underlying surface (MJ/m^3/°C); d_u is the depth of the underlying surface affected by heat conduction (m); T_a is the air temperature on the day of simulation (°C); and T_u is the surface temperature of the underlying surface on the day before simulation (°C).

For soil and SGM layers, the average temperature was represented by the temperature in the middle of the layer. The temperature difference between the atmosphere and the surface is the source of heat conduction; after the heat flux conducted into the snow or soil was determined, the heat flux and temperature of each layer were calculated using the following equation (Shang et al., 1997; Wang et al., 2014):

$$C_v \frac{\partial T}{\partial t} = \frac{\partial}{\partial z}\left[\lambda \frac{\partial T}{\partial z}\right] + L_f \rho_I \frac{\partial \theta_I}{\partial t} \quad (8)$$

where C_v and λ are the volumetric heat capacity (J/[m^3·°C]) and thermal conductivity (W/[m·°C]) of the soil or SGM layer, respectively; L_f is the latent heat of ice melting (3.35×10^5 J/kg); T is the temperature (°C) of the soil or SGM layer; ρ_I is the ice density (kg/m^3); θ_I is the volumetric content of ice in the soil or SGM layer (cm^3/cm^3); z is the layer thickness (m).

For the snow layer added to improve the model, the main water–heat parameters include thermal conductivity, volumetric heat capacity, and snow density. The calculation formulas of each parameter are as follows:

Snow density was calculated via equation (11) (Hedstrom and Pomeroy, 1998):

$$\rho_s = \begin{cases} 67.9 + 51.3e^{T_a/2.6} & T_a \le 0 \\ 119.2 + 20T_a & T_a > 0 \end{cases}. \quad (9)$$

The thermal conductivity and volumetric heat capacity of snow were calculated as follows (Goodrich, 1982; Ling and Zhang, 2006):

$$\lambda_s = \begin{cases} 0.138 - \frac{1.01\rho_s}{1000} + 3.233\left(\frac{\rho_s}{1000}\right)^2 & 156 < \rho_s \le 600 \\ 0.023 + \frac{0.234\rho_s}{1000} & \rho_s \le 156 \end{cases} \text{ and} \quad (10)$$

$$C_{Vs} = 2.09\rho_s \times 10^3, \quad (11)$$

where ρ_s is the snow density (kg/m^3); T_a is the atmospheric temperature (°C); λ_s is the thermal conductivity of the snow (W/[m·°C]); C_{Vs} is the volumetric heat capacity of the snow (J/[m^3·°C]).

As opposed to the uniform soil profile, the presence of gravel also has a great influence on the heat conduction of the soil–gravel layer. The main thermal parameters of the soil–gravel layer include volumetric heat capacity and thermal conductivity. The calculation formulas for each parameter were as follows:

Volumetric heat capacity were calculated via equation (14) (Chen et al., 2008):

$$C_V = (1 - \theta_s) \times C_s + \theta_l \times C_l + \theta_I \times C_I, \quad (12)$$

where θ_s, θ_l, and θ_I are the saturated volumetric water content, volumetric liquid water content, and volumetric ice content of the soil or SGM layer, respectively; C_s, C_l, and C_I are the volumetric heat capacity (J/[m^3·°C]) of the soil or SGM layer, water, and ice, respectively; at 0 °C, the soil and SGM layers have values of 1.93×10^6 J/[m^3·°C] and 3.1×10^6 J/[m^3·°C], respectively; and water and ice have values of 4.213×10^6 J/[m^3·°C] and 1.94×10^6 J/[m^3·°C], respectively.

The thermal conductivity calculation referred to the IBIS model, as follows (Foley et al., 1996):

$$\lambda = \lambda_{st} \times (56^{\theta_l} + 224^{\theta_I}), \text{ and} \quad (13)$$

$$\lambda_{st} = \omega_{gravel} \times 1.5 + \omega_{sand} \times 0.3 + \omega_{silt} \times 0.265 + \omega_{clay} \times 0.25, \quad (14)$$

where λ and λ_{st} are the actual thermal conductivity of the soil or SGM layer and the thermal conductivity in the dry state (W/[m·°C]), respectively, and ω_{gravel}, ω_{sand}, ω_{silt}, and ω_{clay} are the volume ratios of the gravel, sand, silt, and clay, respectively.

2.3 Model evaluation criteria

Data from January 2013 to December 2018 were used to evaluate the simulation results of daily flow rates at Gongbujiangda, Baheqiao, and Duobu stations. The performance of the model was first evaluated using a qualitative assessment via graphs and then assessed quantitatively using statistical metrics including the root mean squared error (RMSE), the Nash–Sutcliffe efficiency (NSE) and relative error (RE). The RMSE, NSE and RE were calculated as follows:

$$RMSE = \sqrt{\frac{1}{N}\sum_{i=1}^{N}[(O_i - S_i)^2]} \quad (15)$$

$$NSE = 1 - \frac{\sum_{i=1}^{N}[(O_i - S_i)^2]}{\sum_{i=1}^{N}(O_i - \overline{O_i})^2} \quad (16)$$

$$RE = \frac{\sum_{i=1}^{N} S_i - \sum_{i=1}^{N} O_i}{\sum_{i=1}^{N} O_i} \times 100\% \quad (17)$$

where N is the number of observations; O_i is the observed value; $\overline{O}$ is the mean observed value; and S_i is the simulated value.

3 Results and discussion

3.1 Model calibration and validation

The Niyang River Basin was divided into 217 sub-basins, and each sub-basin was divided into 1~10 contour bands as the basic calculation unit according to the elevation. The basin was divided into 871 contour bands. The average area of the contour bands is 20 km^2. The sub-basins of the watershed and the division of the contour bands are shown in Appendix A.

We calibrated and verified the daily flow process of Gongbujiangda, Baheqiao, and Duobu stations—located upstream, on the largest tributary, and downstream, respectively—from 2013 to 2018. The data from Duobu station were split into two parts: data from 2013 to 2015, which were used for calibration, while those from 2016 to 2018 were used for validation. The discontinuous, measured flow data from Gongbujiangda and Baheqiao stations from 2013 to 2018 were used to verify the model.

The parameters of the model were divided into four categories namely underlying surface parameters, vegetation parameters, soil parameters and aquifer parameters. All parameters have physical meaning and can be estimated based on observational experimental data or remote sensing data. The sensitivities of the above four types of parameters were analyzed (Jia et al., 2006), and the sensitivities of the parameters were divided into three levels namely high, medium, and low. Highly sensitive parameters included soil thickness, soil saturated hydraulic conductivity, and riverbed material permeability coefficient. These parameters were calibrated with actual measurement, and the results were as follows. The saturated hydraulic conductivity of the soil layer was 0.648 m/d, that of the SGM layer was 4.32 m/d, and the riverbed conductivity was approximately 5.184 m/d. The thicknesses of the soil layers at the mountaintop, mountainside, and foot of the mountain were 0.4 m, 0.6 m, and 1.0 m, respectively. In addition, for model improvement, the main parameter calibration results are as follows: the degree-day factor of snow was 4 mm/[°C·day], the critical temperature of snow melting was −1 °C, and the critical value of non-heavy and heavy rain periods was 15 mm/day.

Figure 5 and Table 1 present the results of both calibration and verification periods of the daily flow data from Duobu station and only the latter from Gongbujiangda and Baheqiao stations. The simulation results of the WEP-QTP model from the three stations were consistent with the measured flow data. During the verification period, compared with the WEP-COR model, the NSE of WEP-QTP increased and the RE decreased, thereby considerably improving the simulation effect of the model. The WEP-QTP simulation flow process was smoother, and a large flow peak was not easily formed. However, we also found that WEP QTP underestimated the river discharge during the frozen period, which may be attributed to the model not

explicitly considering the outflow of sub-permafrost water, which could also supplement the river discharge in the frozen period through the macropores in the bedrock fracture zone. In general, the WEP-QTP model delivered an acceptable performance for the Niyang River Basin and achieved NSE > 0.75 and RE < 10 % for the validation period. The improved model could be used for further analysis.

Table 1: Model validation results for Gongbujiangda, Baheqiao, and Duobu stations

Model	Duobu				Gongbujiangda		Baheqiao	
	Calibration		Validation		Validation		Validation	
	NSE	RE	NSE	RE	NSE	RE	NSE	RE
WEP-QTP	0.89	−5.8 %	0.76	3.4 %	0.79	0.01 %	0.75	−5.47%
WEP-COR	0.69	−4.65%	0.31	0.01 %	0.67	1.66 %	0.40	−2.38 %

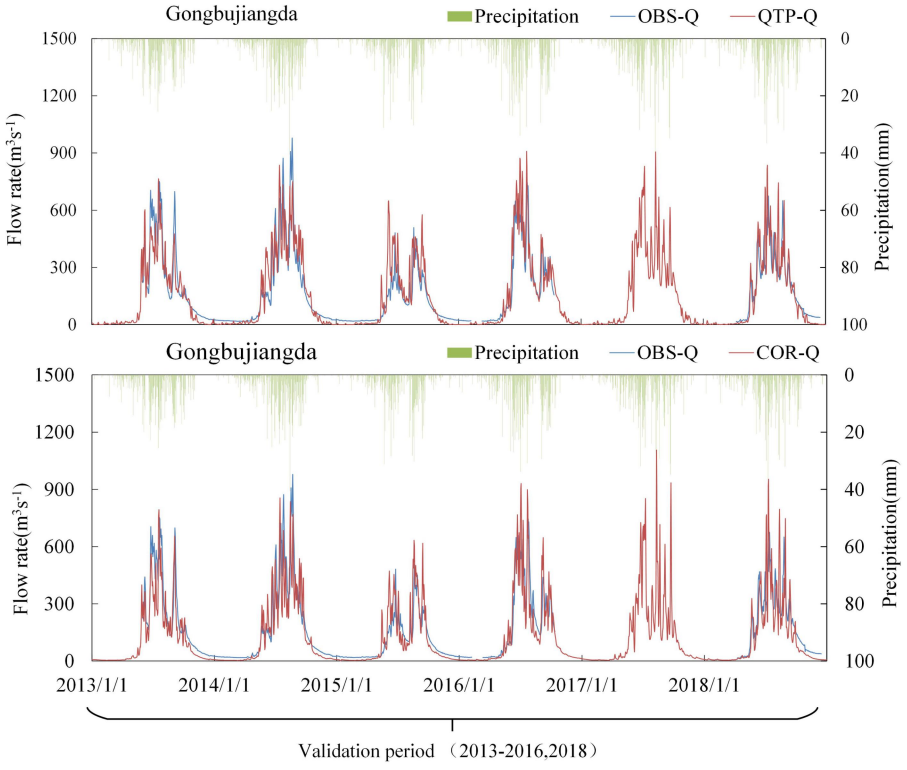

(a)

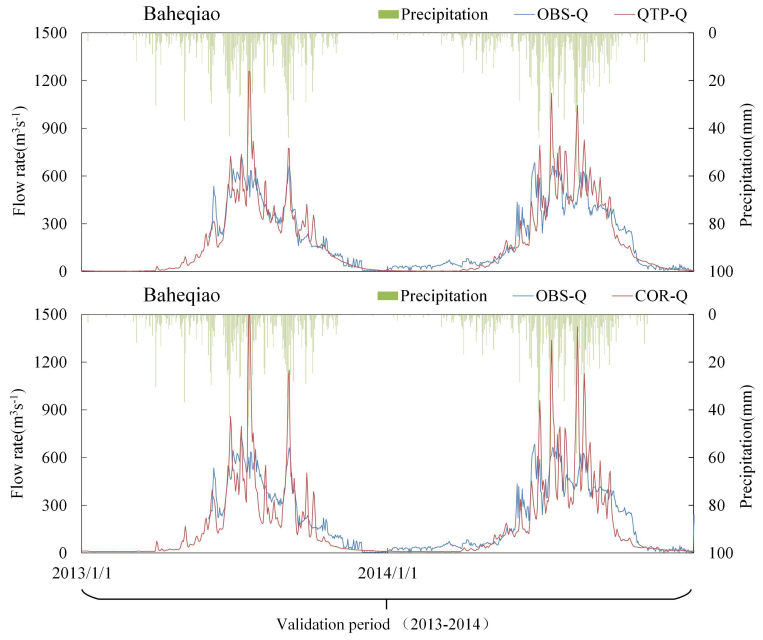

(b)

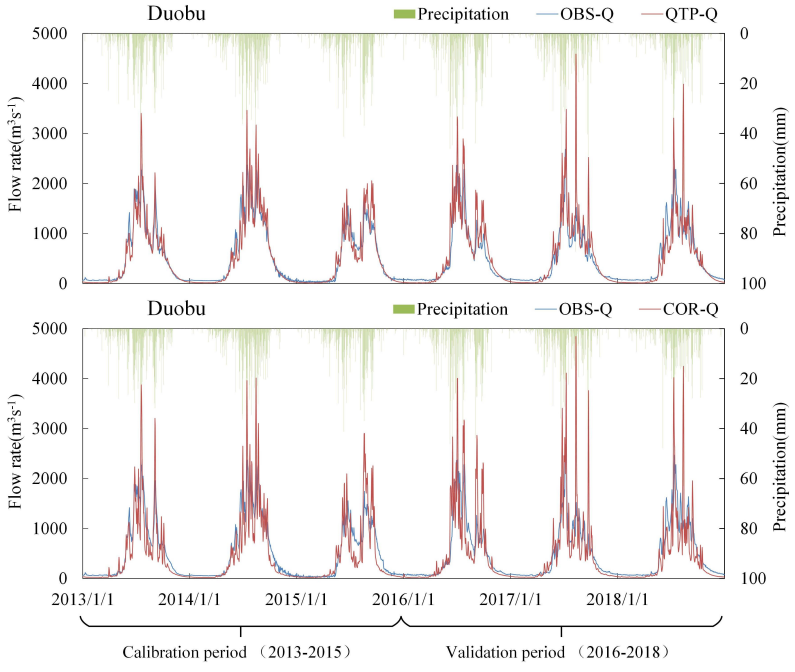

370 (c)

Figure 5: Verification results of the WEP-QTP and WEP-COR models at (a) Duobu, (b) Gongbujiangda, and (c) Baheqiao stations

3.2 Simulation and comparison of soil–gravel water–heat data at test sites

Figure 6 shows the air temperature and the simulated and measured snow thickness during freezing and thawing at the test point. The snow began to accumulate on 3 December 2016 and was completely melted by 4 April 2017. The maximum snow thickness was 12.4 cm, and the simulated snow thickness was consistent with the measured value. The temperature and moisture of the soil–gravel layer at the experimental point during the freezing and thawing period of the soil were compared with the measured results.

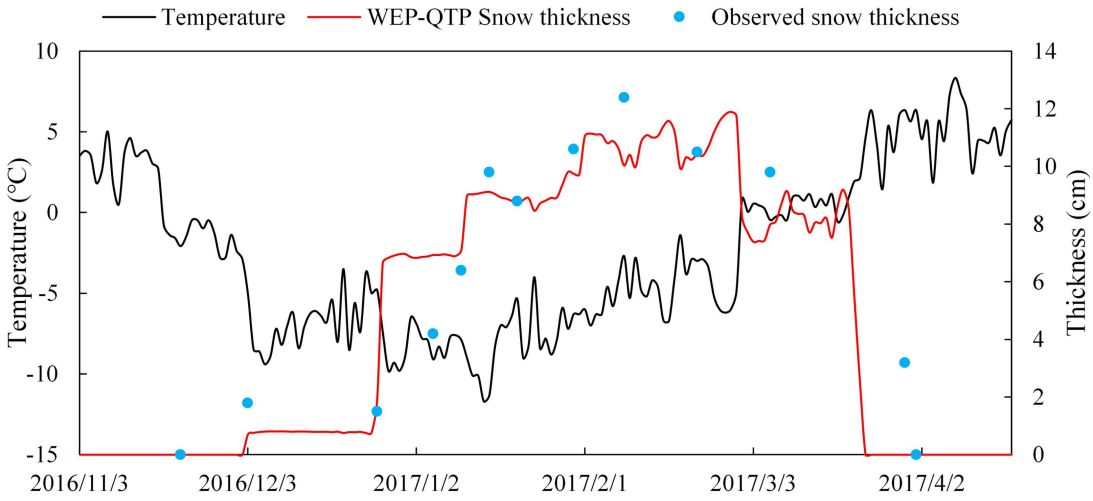

Figure 6: Snow thicknesses and temperatures during freezing and thawing at the experimental sites from observations and the WEP-QTP model simulated results

3.2.1 Soil–gravel temperature

The soil–gravel temperature simulation results of the WEP-QTP and WEP-COR models are shown in Figure 7. The soil thickness at the test site was approximately 40 cm. For the 10 cm layer, because the simulation parameters of the WEP-QTP and WEP-COR models were the same, the temperature simulation results were consistent except for the snow cover period (i.e., the period when the snow thickness was > 5 cm, 27 December 2016–20 March 2017). Due to the insulation effect of snow, the heat transfer and temperature fluctuations of the surface soil were reduced. The RMSE of WEP-QTP in the 10 cm soil layer was 1.09 °C during the snow cover period, which was much less than the 2.12 °C of WEP-COR. The simulation results of the two models in the 20 cm layer did not differ considerably. For the 40 cm layer and below, the soil in the WEP-COR had a higher water content than the SGM in the WEP-QTP at the early stage of freezing, masking the difference in simulated temperature between the two models (the volumetric heat capacity of water is greater than that of gravel and soil). However, as the temperature decreased, the moisture in the soil was converted into ice with a smaller heat capacity; thus, the difference in thermodynamic properties between the SGM and the soil increased gradually. During this period, the simulation difference between the two models reached a maximum of 1.41 °C (40 cm layer, 26 January 2017).

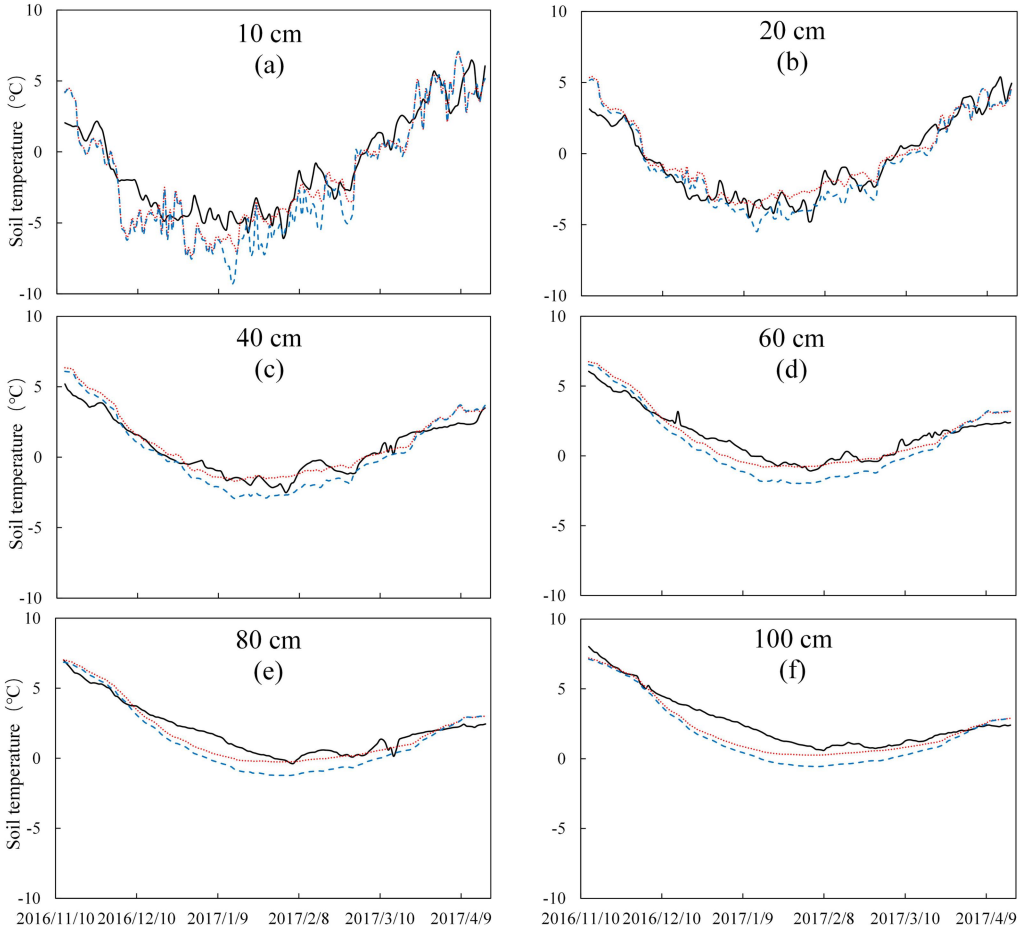

Figure 7: Simulated (WEP-QTP and WEP-COR models) and observed temperatures of the soil–gravel layer at different depths

We also compared the simulation results of the scenario considering only SGM (SGM Scenario) and the scenario considering only snow cover (SC Scenario) to quantitatively analyze how snow and gravel affect the simulation results (Table 2). From the Table 2 it can be found that for the average RMSE: WEP-QTP < SGM Scenario < SC Scenario < WEP-COR. Compared to the WEP-COR model, both snow and SGM improved the accuracy of temperature simulation, but the location of their main effects on heat transfer was different. The RMSE of SC Scenario in the 10-20 cm layers was smaller than that of SGM Scenario. The snow cover reduces the heat transfer and temperature fluctuations of the surface layer, which improves the simulation accuracy of the surface soil temperature. For layers of 40 cm and below, the RMSE of the SGM Scenario was smaller than that of the SC Scenario, and the influence of SGM was dominant. Overall, the addition of the snow layer reduces the temperature fluctuations in the top soil and in conjunction with the SGM layer, corrects the original model's overestimation of the freeze-thaw rate. The temperature RMSE was reduced from 1.16 °C to 0.86 °C.

Table 2 RMSE values for the soil temperature simulation (°C)

Depth (cm)	WEP-QTP	WEP-COR	SGM Scenario	SC Scenario
10	1.53	1.89	1.79	1.64
20	1.00	0.93	0.95	0.88
40	0.63	0.87	0.65	0.75
60	0.59	1.03	0.65	0.92
80	0.63	1.06	0.70	0.96
100	0.79	1.20	0.87	1.12
Mean	0.86	1.16	0.94	1.05

3.2.2 Soil–gravel moisture

Figure 8 shows a comparison between the simulated and measured values of the liquid water content in the freeze–thaw period of the WEP-QTP and WEP-COR models at the experimental points in 2016–2017. During the freezing period (December–March), the upper layer liquid water content first dropped due to the temperature drop, followed by liquid water content drop in the lower SGM layer, which stabilized in January–February. When the temperature increased in March, the upper layer initially began to melt, thereby increasing the liquid water content and the subsequent melting of the lower layer. At the end of freeze–thaw period, the upper part of the soil–gravel layer had a higher water content than that in the lower part due to the infiltration of snow melt, and was also higher than before freezing.

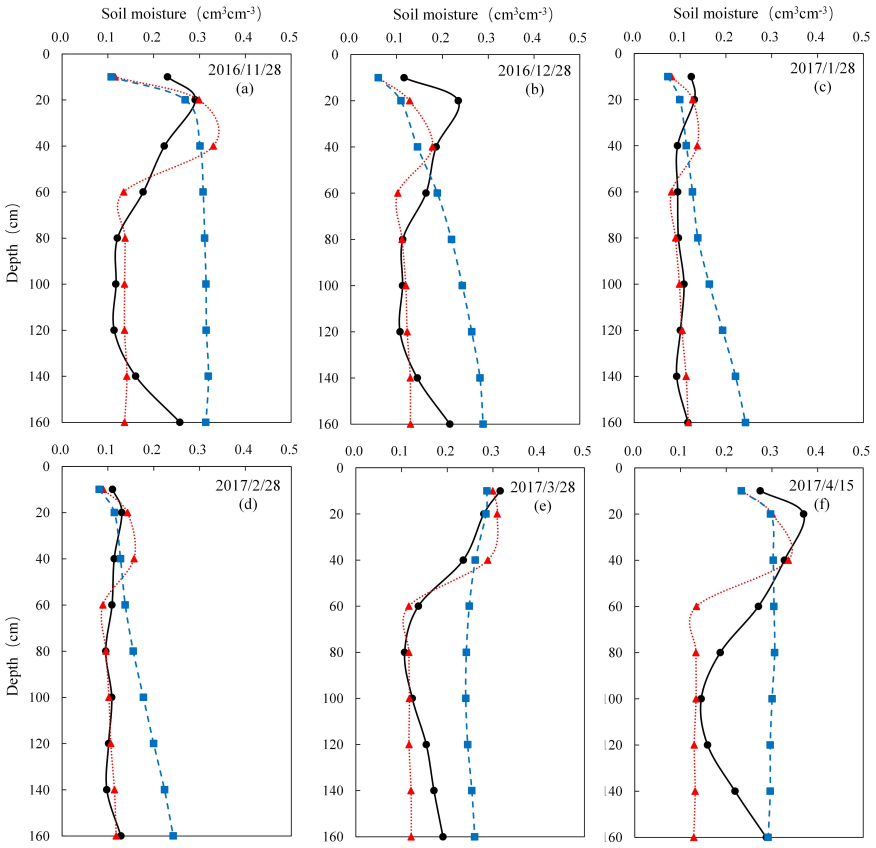

Figure 8: Simulated (WEP-QTP and WEP-COR models) and observed moisture contents of the soil–gravel layer during the freezing and thawing periods

During the entire freeze–thaw period, the lower SGM layer did not affect the simulation of soil moisture content in the 10 cm layer; For the 20–40 cm soil layers, their water holding capacity in the WEP-QTP model was greater than that of the SGM layer under it, so that the moisture simulated by the WEP-QTP model was greater than that of the WEP-COR model; Below 40 cm, the simulation difference between the two models starts to emerge clearly. The simulated moisture of the WEP-COR model changed gradually in the vertical direction and was greater than the measured value. While the moisture simulated by the WEP-QTP model was lower and closer to the measured value. This was attributed to the fact that the thickness of the soil layer at the experimental site was 40 cm, and below it is the SGM layer with higher hydraulic conductivity and lower water holding capacity. The WEP-COR model did not take into account the influence of the layered geological features on water migration. However, as the actual condition of the underlying surface cannot be homogeneous like in the model generalization, there was a discrepancy in the model simulation results. Soil with low gravel content may be present near the 160 cm layer. In March and April after the snow melts, the snowmelt water infiltrates to this layer and was more likely to reside there, and the measured values of this layer was between the simulated values of the WEP-QTP and WEP-COR. The

average RE of WEP-COR was 33.74%, and that of WEP-QTP was smaller at -12.11%. WEP-QTP could reflect the influence of gravel on the vertical migration of water.

3.3 Simulation and comparison of watershed flow process

To further analyze the improved WEP-QTP compared with the original WEP-COR, three sites with data for 2014 were selected, and the daily flow data of the three stations were compared with the simulated data of the two models (Fig. 9). The simulation difference between the two models was from June to October. Compared to the whole year, the difference between the RMSE of the two models was the largest from June to September, and the difference between the RE of the two models was the largest in October (Table 3). For stations Gongbujiangda, Baheqiao and Duobu, the RMSEs of WEP-QTP decreased by 14.44 m^3/s, 62.81 m^3/s, and 149.12 m^3/s, respectively, from June to September, and the absolute values of RE decreased by 4.08 %, 32.67 %, and 45.50 %, respectively, in October. The simulation performance of the WEP-QTP was better than that of the WEP-COR in three aspects: the peak value of the flood season was not too high; the valley value of the flow process was higher than that of the WEP-COR; better showed a observed "tailing" process after September.

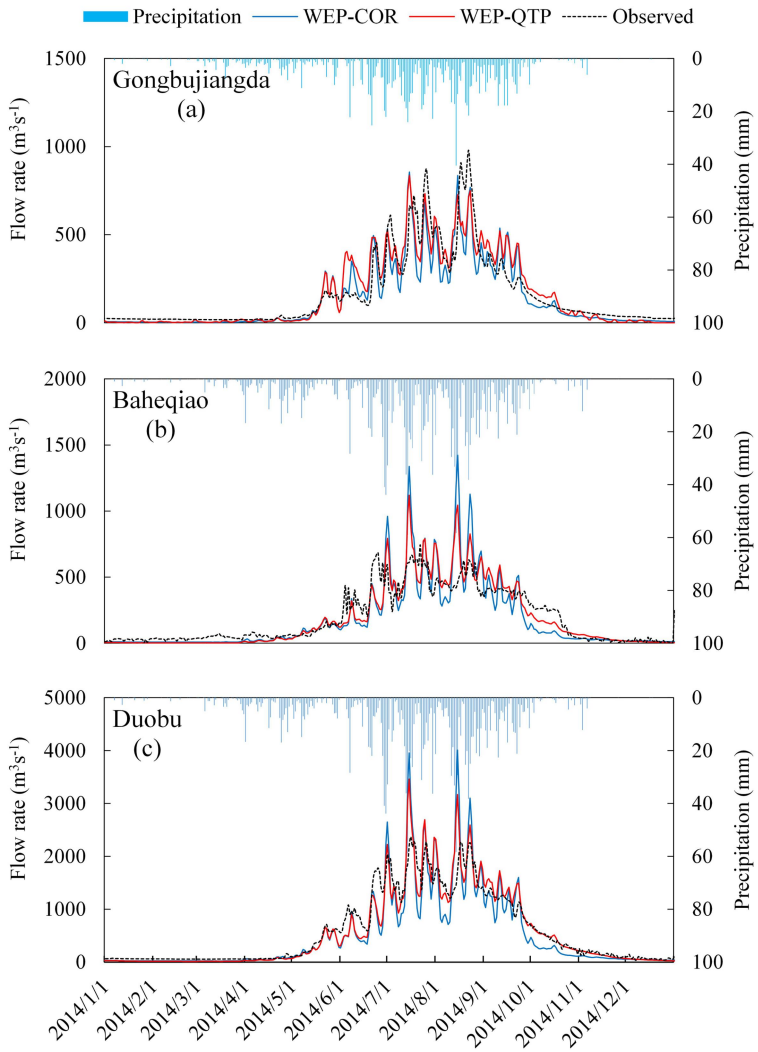

Figure 9: Simulated (WEP-QTP and WEP-COR models) and observed flow rates at (a) Gongbujiangda, (b) Baheqiao, and (c) Duobu stations in 2014

Table 3 Statistical values of WEP-QTP and WEP-COR models for soil temperature simulation in different periods

Statistical value	Gongbujiangda		Duobu		Baheqiao	
	WEP-QTP	WEP-COR	WEP-QTP	WEP-COR	WEP-QTP	WEP-COR
RMSE (m^3/s)	88.47/ 148.32/35.99[a]	96.27/ 162.76/30.19	106.48/ 175.61/79.05	145.05/ 238.42/140.55	244.39/ 416.74/45.64	335.56/ 565.86/211.33
RE (%)	2.20/7.78/19.86	13.12/8.72/23.94	-1.95/7.06/-31.72	7.29/-3.06/64.39	-3.78/-0.11/1.25	12.71/7.31/46.76

[a] Values of the whole year, June to September, and October, respectively.

Figure 10 shows the comparison and analysis of the changes in hydrological cycle flux simulated by WEP-QTP and WEP-COR. From June to September, the surface runoff from precipitation simulated by WEP-QTP decreased by 31.79% when compared with WEP-COR; correspondingly, groundwater recharge and groundwater discharge increased by 249.16% and 280.41%, respectively. The precipitation in WEP model can recharge groundwater more rapidly during heavy rains through macropores in the SGM layer, while flow peaks are not easily formed. However, in the WEP-COR model, this part of water mostly formed the peak flow during the flood season, which far exceeded the measured value of the flow (Fig. 9). Therefore, the WEP-QTP performed better in the peak simulation during the flood season, and could simulate more groundwater discharge to river, so that it performed better when simulating low-flow.

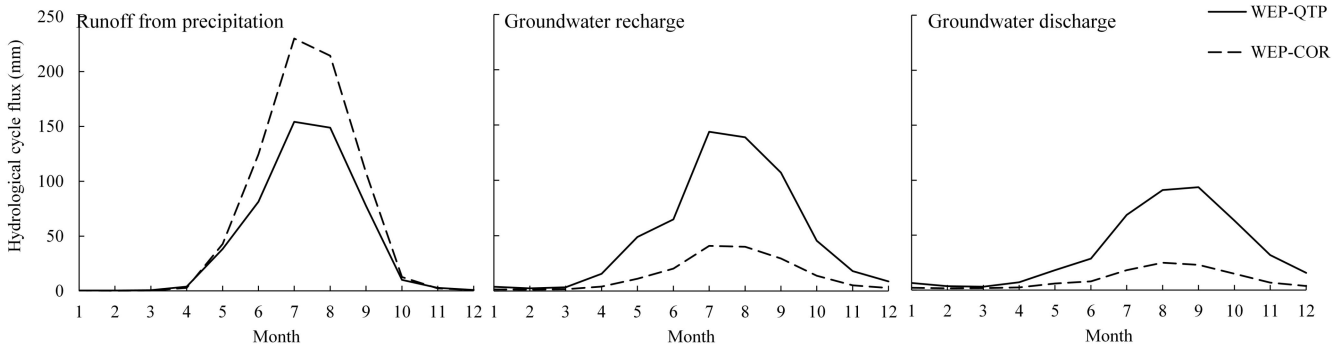

Figure 10: Monthly change process of hydrological cycle flux simulated by WEP-QTP and WEP-COR

The addition of the snow layer not only reduced the temperature fluctuation of the surface soil, but also, with the help of the SGM layers, revised the original model's overestimation of the freeze-thaw speed. In the lower elevation valleys (< 4,600 m a.s.l.), the percentage of area with snow thickness greater than 0.5 m reached its maximum (18.36%) in February and then decreased to 0 % by June. However, in the high-altitude area (> 4,600 m a.s.l.), where the temperature was lower than that in the valley, the percentage of area with snow thickness greater than 0.5 m reached its maximum (51.26%) in April and then dropped to a minimum of 0.60% in July (Fig. 11). The WEP-COR did not consider snow cover, the upper boundary was the atmosphere, and the soil responds quickly to the change of atmospheric temperature. During the thawing process, the frozen soil area and the area with frozen thickness greater than 1 m decreased and then increased with temperature from January to December (maximum in January, minimum in August). In contrast, the proportion of area with frozen soil thickness > 1.5 m simulated by the WEP-QTP reached the maximum in February and the minimum in September (Fig. 12). The inconsistency in spatial and temporal variation of the frozen soil led to discrepancies in groundwater recharge and discharge processes in the two models. The frozen soil area change simulated by the WEP-QTP lagged that of the WEP-COR, as well as the groundwater discharge process (QTP's groundwater discharge reached its maximum in September, while that of COR was in August (Fig. 10)). Water in the WEP-QTP model had more time for groundwater recharge and river recharge, thus showing a better observed "tailing" process compared with the WEP-COR.

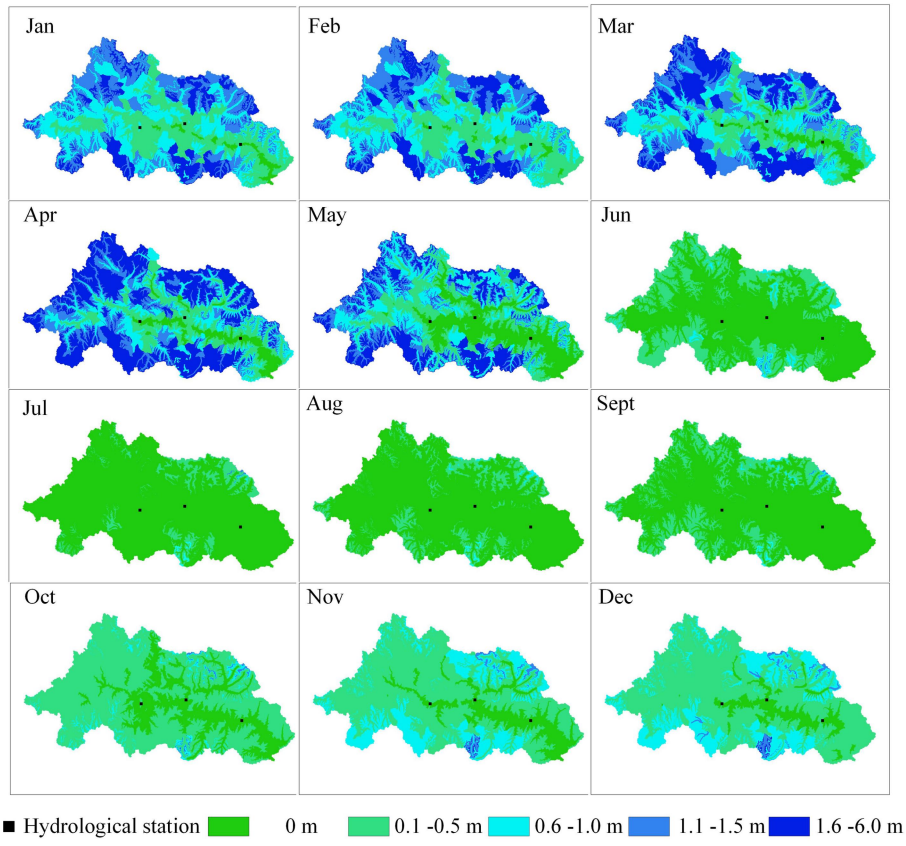

475 **Figure 11. Temporal and spatial variation of snow cover thickness in 2014**

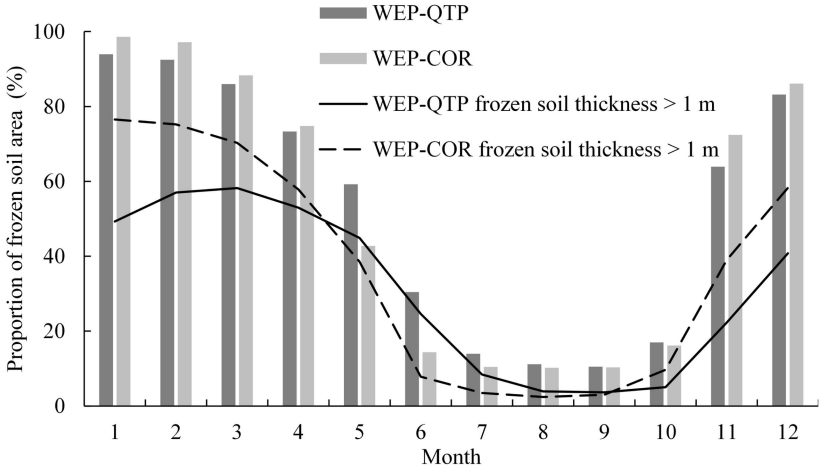

Figure 12: Monthly change process of the frozen soil area proportion in the basin

In cold regions, climate change affects high and low flows differently. As the warming and wetting continue, changes in high flows show spatial heterogeneity, while low flow shows a consistent increasing trend (Song et al., 2021). Warming enhances subsurface flow connectivity and increases groundwater flow by increasing the thickness of the active layer (St. Jacques and Sauchyn, 2009; Walvoord and Kurylyk, 2016). As the medium connecting groundwater and surface water, the water–heat transport of the active layer has a great influence on the water cycle process in cold regions (Chen et al., 2014; Kurylyk et al., 2014). Our study demonstrates that the soil–gravel layer structure in the QTP is different from the soil layer structure in general cold regions. In terms of heat transfer, snow and gravel block heat conduction and slow down the freezing and thawing rates of aquifers. For water transfer, the large pores of the lower SGM layer increase the regulation and storage effect of groundwater of the flow processes. Under the future climate conditions, the participation of groundwater in the water cycle of the QTP may be higher than we expected. Ignoring the snow–soil–gravel layer structure will affect the hydrological forecast, reservoir regulation, and water resource utilization.

4 Conclusions

This study combined the geological characteristics of the thin soil layer on the thick SGM layer and the climate characteristics of the long snow cover period in the QTP. Using the Niyang River Basin as the research area, the WEP-QTP model was constructed based on the original WEP-COR model. The improved model divides the uniform soil profile into two types of media: the upper soil and the lower SGM. When no phase change occurs in the ground, two infiltration models based on the dualistic soil–gravel structure were developed based on the Richards equation in non-heavy rain scenarios and the multi-layer Green–Ampt model in heavy rain scenarios. During the freeze–thaw period, a water–heat coupling model based on the snow–soil–gravel continuum was constructed. This model was used to simulate the water cycle processes of the Niyang River Basin, and the improvement effect of the model was analyzed via comparison with the WEP-COR.

Compared with the simulation results prior to improvement, the addition of snow not only reduced the surface soil temperature fluctuations, but also interacted with the SGM layer to reduce the soil freezing and thawing speed. The low estimation of temperature by WEP-COR was corrected, while the temperature RMSE was reduced from 1.16 °C to 0.86 °C. At the same time, the WEP-QTP model can reflect the impact of the SGM layer under the soil on the vertical movement of water and accurately describe the dynamic changes in moisture in the soil and SGM layers; the RE of the moisture content was reduced from 33.74% to −12.11%.

According to the comparison of the WEP-QTP simulation and measured results of the main stations in the Niyang River Basin, the daily flow process simulated by the model is in line with the actual status, while the flow simulation result was more accurate (Nash > 0.75 and $|RE| < 10$ %), which is a considerable improvement compared with the WEP-COR model. In the fully thawed period, the dualistic soil–gravel structure increased the recharge and discharge of groundwater and improved the regulation effect of groundwater on flow, thereby stabilizing the water flow process. The maximum RE at the flow peak and valley decreased by 88.2% and 21.3%, respectively. In the freeze–thaw period, by considering the effect of

the snow–soil–gravel layer continuum on soil freezing and thawing processes, changes in frozen soil depth simulated by WEP-QTP lagged those of WEP-COR by approximately one month. There was more time for the river recharge by the groundwater, which showed a better observed "tailing" process after September.

In contrast to the general cold area, the unique geological structure and climatic characteristics of the QTP change the water cycle processes in the basin. Ignoring the influence of the dualistic soil–gravel structure greatly impacts the hydrological forecast and water resource assessment.

Data and code availability

The datasets and model code relevant to the current study are available from the corresponding author on reasonable request.

Author contribution

PW performed the model programming and simulations. ZZ, KW and YL conducted the field experiments. ZZ, JL, YL, and JL contributed to the model programming. PW and ZZ performed the writing. CX, YJ and HW contributed to the writing of the paper.

Competing interests

The authors declare that they have no conflict of interest.

Acknowledgements

This work was partly supported by grants from the National Natural Science Foundation of China (91647109, 51879195) and the National Key Research and Development Program of China (2016YFC0402405).

References

Arocena, J., Hall, K., and Zhu, L. P.: Soil formation in high elevation and permafrost areas in the Qinghai Plateau (China), Spanish Journal of Soil Science, 2, 34-49, 2012.

Beibei, Z., Ming'an, S., and Hongbo, S.: Effects of rock fragments on water movement and solute transport in a Loess Plateau soil, Comptes Rendus Geoscience, 341, 462-472, 2009.

Chen, B., Luo, S., Lü, S., Zhang, Y., and Ma, D.: Effects of the soil freeze-thaw process on the regional climate of the Qinghai-Tibet Plateau, Climate research, 59, 243-257, 2014.

Chen, H., Nan, Z., Zhao, L., Ding, Y., Chen, J., and Pang, Q.: Noah modelling of the permafrost distribution and characteristics in the West Kunlun area, Qinghai - Tibet Plateau, China, Permafrost and Periglacial Processes, 26, 160-174, 2015.

Chen, R.-s., Lu, S.-h., Kang, E.-s., Ji, X.-b., Zhang, Z., Yang, Y., and Qing, W.: A distributed water-heat coupled model for mountainous watershed of an inland river basin of Northwest China (I) model structure and equations, Environmental Geology, 53, 1299-1309, 2008.

Cheng, G. and Wu, T.: Responses of permafrost to climate change and their environmental significance, Qinghai-Tibet Plateau, Journal of Geophysical Research: Earth Surface, 112, 2007.

Cheng, G. and Jin, H.: Permafrost and groundwater on the Qinghai-Tibet Plateau and in northeast China, Hydrogeology Journal, 21, 5-23, 2013.

Cherkauer, K. A. and Lettenmaier, D. P.: Simulation of spatial variability in snow and frozen soil, Journal of Geophysical Research: Atmospheres, 108, 2003.

Childs, S. W. and Flint, A. L.: Physical properties of forest soils containing rock fragments, Forestry Publications, 95-121, 1990.

Cousin, I., Nicoullaud, B., and Coutadeur, C.: Influence of rock fragments on the water retention and water percolation in a calcareous soil, Catena, 53, 97-114, 2003.

Dai, L., Guo, X., Zhang, F., Du, Y., Ke, X., Li, Y., Cao, G., Li, Q., Lin, L., and Shu, K.: Seasonal dynamics and controls of deep soil water infiltration in the seasonally-frozen region of the Qinghai-Tibet plateau, Journal of Hydrology, 571, 740-748, 2019.

Deng, D., Wang, C., and Peng, P.: Basic Characteristics and Evolution of Geological Structures in the Eastern Margin of the Qinghai-Tibet Plateau, Earth Sciences Research Journal, 23, 283-291, 2019.

Ding, Y., Zhang, S., Wu, J., Zhao, Q., Li, X., and Qin, J.: Recent progress on studies on cryospheric hydrological processes changes in China, Advances in Water Science, 31(5), 690-702, 2020.

Douville, H., Royer, J.-F., and Mahfouf, J.-F.: A new snow parameterization for the Meteo-France climate model, Climate Dynamics, 12, 21-35, 1995.

Dutra, E., Viterbo, P., Miranda, P. M., and Balsamo, G.: Complexity of snow schemes in a climate model and its impact on surface energy and hydrology, Journal of Hydrometeorology, 13, 521-538, 2012.

Foley, J. A., Prentice, I. C., Ramankutty, N., Levis, S., Pollard, D., Sitch, S., and Haxeltine, A.: An integrated biosphere model of land surface processes, terrestrial carbon balance, and vegetation dynamics, Global biogeochemical cycles, 10, 603-628, 1996.

Franzluebbers, A. J.: Water infiltration and soil structure related to organic matter and its stratification with depth, Soil and Tillage research, 66, 197-205, 2002.

Goodrich, L. E.: The influence of snow cover on the ground thermal regime, Canadian geotechnical journal, 19, 421-432, 1982.

Grinsted, A.: An estimate of global glacier volume, The Cryosphere, 7, 141, 2013.

Hedstrom, N. and Pomeroy, J.: Measurements and modelling of snow interception in the boreal forest, Hydrological Processes, 12, 1611-1625, 1998.

Hock, R.: A distributed temperature-index ice-and snowmelt model including potential direct solar radiation, Journal of Glaciology, 45, 101-111, 1999.

Hu, Z., Islam, S.: Prediction of ground surface temperature and soil moisture content by the force - restore method. Water Resources Research, 31(10): 2531-2539, 1995.

Huyan, Y., Yao, W., Xie, X., and Wang, L.: Provenance, source weathering, and tectonics of the Yarlung Zangbo River overbank sediments in Tibetan Plateau, China, using major, trace, and rare earth elements, Geological Journal, 57, 37-51, 2022.

Ireson, A., Van Der Kamp, G., Ferguson, G., Nachshon, U., and Wheater, H.: Hydrogeological processes in seasonally frozen northern latitudes: understanding, gaps and challenges, Hydrogeology Journal, 21, 53-66, 2013.

Jansson, P. and Karlberg, L.: Coupled heat and mass transfer model for soil-plant-atmosphere systems, Royal Institute of Technology, Dept of Civil and Environmental Engineering, Stockholm, 2011.

Jia, Y. and Tamai, N.: Integrated analysis of water and heat balances in Tokyo metropolis with a distributed model, Journal of Japan Society of Hydrology and Water Resources, 11, 150-163, 1998.

Jia, Y., Ding, X., Qin, C., and Wang, H.: Distributed modeling of landsurface water and energy budgets in the inland Heihe river basin of China, Hydrology and Earth System Sciences, 13, 1849, 2009.

Jia, Y., Ni, G., Kawahara, Y., and Suetsugi, T.: Development of WEP model and its application to an urban watershed, Hydrological Processes, 15, 2175-2194, 2001.

Jia, Y., Wang, H., Zhou, Z., Qiu, Y., Luo, X., Wang, J., Yan, D., and Qin, D.: Development of the WEP-L distributed hydrological model and dynamic assessment of water resources in the Yellow River basin, Journal of Hydrology, 331, 606-629, 2006.

Kurylyk, B. L., MacQuarrie, K. T., and McKenzie, J. M.: Climate change impacts on groundwater and soil temperatures in cold and temperate regions: Implications, mathematical theory, and emerging simulation tools, Earth-Science Reviews, 138, 313-334, 2014.

Larsbo, M., Holten, R., Stenrød, M., Eklo, O. M., and Jarvis, N.: A Dual-Permeability Approach for Modeling Soil Water Flow and Heat Transport during Freezing and Thawing, Vadose Zone Journal, 18, 2019.

Li, J., Zhou, Z., Wang, H., Liu, J., Jia, Y., Hu, P., and Xu, C.-Y.: Development of WEP-COR model to simulate land surface water and energy budgets in a cold region, Hydrology Research, 50, 99-116, 2019.

Li, Z., Yu, G., Xu, M., Hu, X., Yang, H., and Hu, S.: Progress in studies on river morphodynamics in Qinghai-Tibet Plateau. Advances in Water Science, 27(4): 617-628, 2016.

Ling, F. and Zhang, T.: Sensitivity of ground thermal regime and surface energy fluxes to tundra snow density in northern Alaska, Cold regions science and technology, 44, 121-130, 2006.

Liu, X., Yang, W., Zhao, H., Wang, Y., and Wang, G.: Effects of the freeze-thaw cycle on potential evapotranspiration in the permafrost regions of the Qinghai-Tibet Plateau, China, Science of the total environment, 687, 257-266, 2019.

Lundberg, A., Ala-Aho, P., Eklo, O., Klöve, B., Kværner, J., and Stumpp, C.: Snow and frost: implications for spatiotemporal infiltration patterns–a review, Hydrological processes, 30, 1230-1250, 2016.

MAO, X.-m. and SHANG, S.-h.: Method of minimum flux in saturation layer for calculating stable water infiltration through layered soil, Journal of Hydraulic Engineering, 7, 2010.

Mehuys, G., Stolzy, L., Letey, J., and Weeks, L.: Effect of stones on the hydraulic conductivity of relatively dry desert soils, Soil Science Society of America Journal, 39, 37-42, 1975.

Monteith, J.,: Principles of environmental physics Edward Arnold. London, 214p, 1973.

Mualem, Y.: Hydraulic conductivity of unsaturated soils: Prediction and formulas. Methods of Soil Analysis: Part 1 Physical and Mineralogical Methods, 5: 799-823, 1986.

Pan, Y., Lyu, S., Li, S., Gao, Y., Meng, X., Ao, Y., and Wang, S.: Simulating the role of gravel in freeze–thaw process on the Qinghai–Tibet Plateau, Theoretical and applied climatology, 127, 1011-1022, 2017

Pitman, A., Yang, Z., and Henderson-Sellers, A.: Description of bare essentials of surface transfer for the Bureau of Meteorology Research Centre AGCM, Bureau of Meteorology1991.

Pomeroy, J., Gray, D., Brown, T., Hedstrom, N., Quinton, W., Granger, R., and Carey, S.: The cold regions hydrological process representation and model: A platform for basing model structure on physical evidence, Hydrological Processes, 21, 2650-2667, 2007.

Radić, V. and Hock, R.: Regional and global volumes of glaciers derived from statistical upscaling of glacier inventory data, Journal of Geophysical Research: Earth Surface, 115, 2010.

Rigon, R., Bertoldi, G., and Over, T. M.: GEOtop: A distributed hydrological model with coupled water and energy budgets, Journal of Hydrometeorology, 7, 371-388, 2006.

Shang, S.-h., Lei, Z., and Yang, S.: Numerical simulation improvement of coupled moisture and heat transfer during soil freezing, JOURNAL-TSINGHUA UNIVERSITY, 37, 62-64, 1997.

Song, C., Wang, G., Sun, X., and Hu, Z.: River runoff components change variably and respond differently to climate change in the Eurasian Arctic and Qinghai-Tibet Plateau permafrost regions, Journal of Hydrology, 601, 126653, 2021.

St. Jacques, J. M. and Sauchyn, D. J.: Increasing winter baseflow and mean annual streamflow from possible permafrost thawing in the Northwest Territories, Canada, Geophysical Research Letters, 36, 2009.

Sun, H., The formation and evolution of the Qinghai-Tibet Plateau. Shanghai Science and Technology Press, 1996.

Van Genuchten, M. T.: A closed-form equation for predicting the hydraulic conductivity of unsaturated soils, Soil science society of America journal, 44, 892-898, 1980.

Walvoord, M. A. and Kurylyk, B. L.: Hydrologic impacts of thawing permafrost—A review, Vadose Zone Journal, 15, 2016.

Wang, A., Xie, Z., Feng, X., Tian, X., and Qin, P.: A soil water and heat transfer model including changes in soil frost and thaw fronts, Science China Earth Sciences, 57, 1325-1339, 2014.

Wang, H., Xiao, B., and Wang, M.: Modeling the soil water retention curves of soil-gravel mixtures with regression method on the Loess Plateau of China, PLoS One, 8, e59475, 2013.

Wang, Y., Yang, H., Yang, D., Qin, Y., Gao, B., and Cong, Z.: Spatial interpolation of daily precipitation in a high mountainous watershed based on gauge observations and a regional climate model simulation, Journal of Hydrometeorology, 18, 845-862, 2017.

Watanabe, K. and Kugisaki, Y.: Effect of macropores on soil freezing and thawing with infiltration, Hydrological Processes, 31, 270-278, 2017.

Yang, K., Chen, Y.-Y., and Qin, J.: Some practical notes on the land surface modeling in the Tibetan Plateau, Hydrology and Earth System Sciences, 13, 687-701, 2009.

Yi, S., Chen, J., Wu, Q., and Ding, Y.: Simulating the role of gravel on the dynamics of permafrost on the Qinghai-Tibetan Plateau, The Cryosphere Discussions, 7, 4703-4740, 2013.

Yu, L., Feng C.: Recent progress in climate change over Tibetan Plateau. Plateau and Mountain Meteorology Research, 32(3): 84-88, 2012.

Zaradny, H.: Groundwater flow in saturated and unsaturated soil. Balkema Press, Rotterdam, 1993.

Zhang, Y., Cheng, G., Li, X., Han, X., Wang, L., Li, H., Chang, X., and Flerchinger, G.: Coupling of a simultaneous heat and water model with a distributed hydrological model and evaluation of the combined model in a cold region watershed, Hydrological Processes, 27, 3762-3776, 2013.

Zhang, Z. F., Ward, A. L., and Keller, J. M.: Determining the porosity and saturated hydraulic conductivity of binary mixtures, Vadose Zone Journal, 10, 313-321, 2011.

Appendix A Distribution of major hydrologically-relevant features in the basin

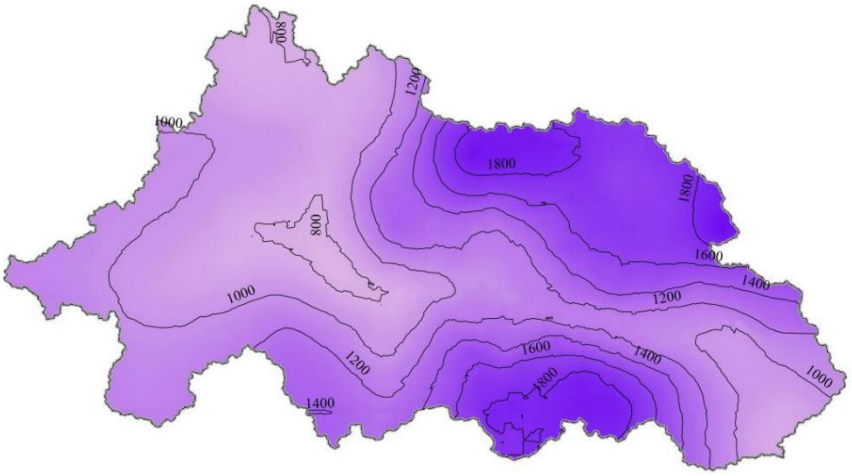

Figure A1. Annual precipitation contour map (mm/year).

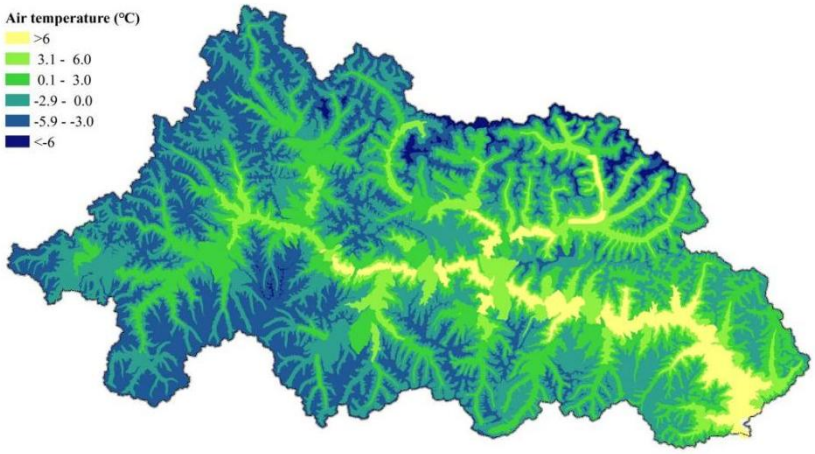

660

Figure A2. Mean annual temperature (°C).

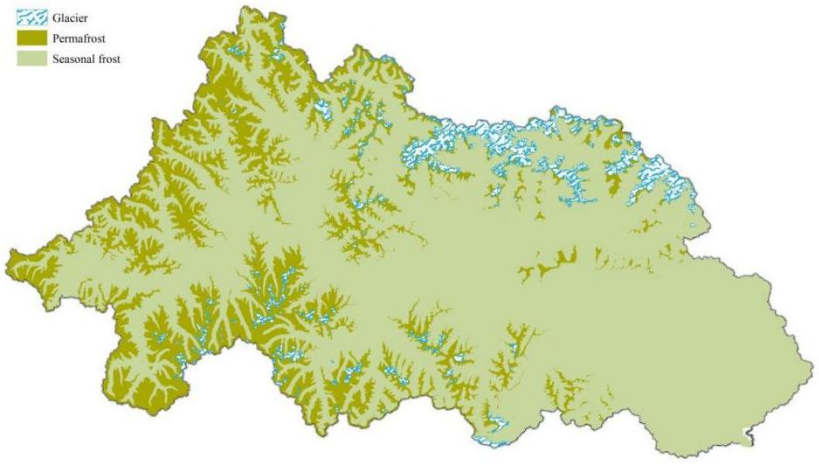

Figure A3. Glacier and permafrost distributions.

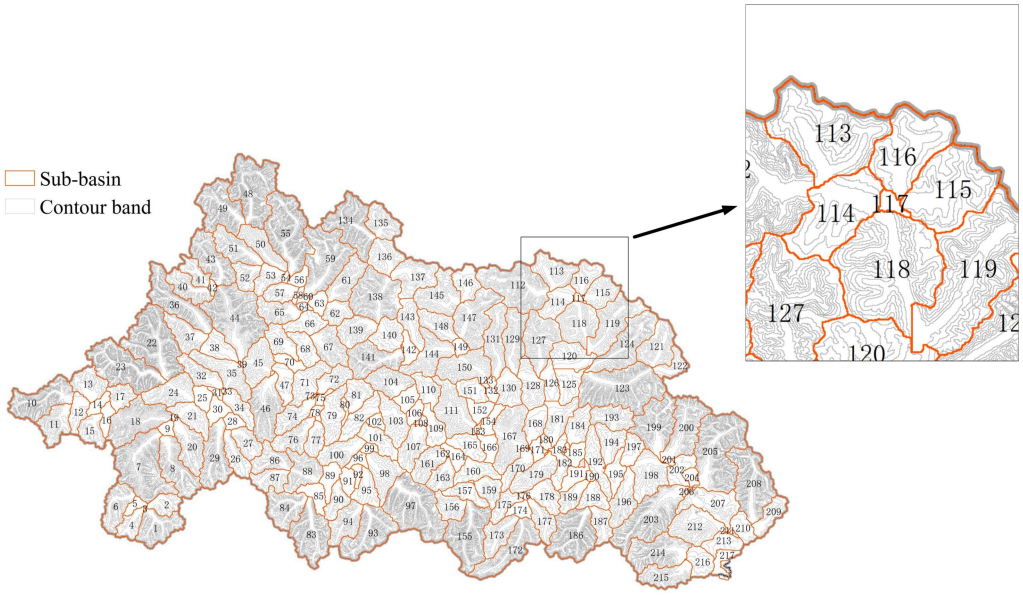

Figure A4. The division of the contour bands

Appendix B Introduction of WEP-COR model

The WEP-QTP model was developed based on the Water and Energy transfer Processes in Cold Regions (WEP-COR) model. For better understanding and comparison, the WEP-COR model is briefly introduced in this section.

Model structure

The WEP-COR model is a distributed hydrological model. In terms of the horizontal structure, the WEP-COR uses the contour bands inside small sub-basins as the basic calculation unit (Fig. B1a), and fully considers the vertical changes in vegetation, soil, air temperature, precipitation, and other factors in the basin with elevation. Each unit is divided into five types according to the land-use type: water body, soil–vegetation, irrigated farmland, non-irrigated farmland, and impervious area. The calculation result of the water and heat flux in each type was weighted by area to obtain the water and heat flux of the contour band. Evapotranspiration of water and soil was calculated using the Penman formula, and the vegetation canopy evaporation was calculated using the Penman–Monteith formula (Monteith, 1973). For soil moisture, the Green–Ampt infiltration model was used during the heavy rain period (Jia and Tamai, 1998), and the non-heavy rain period was simulated by the Richards equation (Jia et al., 2009). The subsurface runoff was calculated based on slope and soil hydraulic conductivity, and groundwater movement was calculated by the Boussinesq's equation (Zaradny, 1993). For glacier-covered areas, the "degree-day factor method" (Hock, 1999) was used to calculate the quantity of glacier melting, and the runoff from the melting of glaciers was directly added to the corresponding hydrological calculation unit.

The vertical structure of WEP-COR was divided into the vegetation canopy or building interception layer, the surface depression storage layer, the aeration layer, the transition zone layer, and the groundwater layer. To accurately simulate the changes in soil moisture and heat from the surface to the deep layers and to reflect the influence of soil depth on the evaporation of bare soil and the water absorption and transpiration of vegetation roots, the aerated zone soil was divided into 11 layers (Fig. B1b). The thickness of the first and second layers was set to 10 cm, and the thickness of layers 3–11 was set to 20 cm.

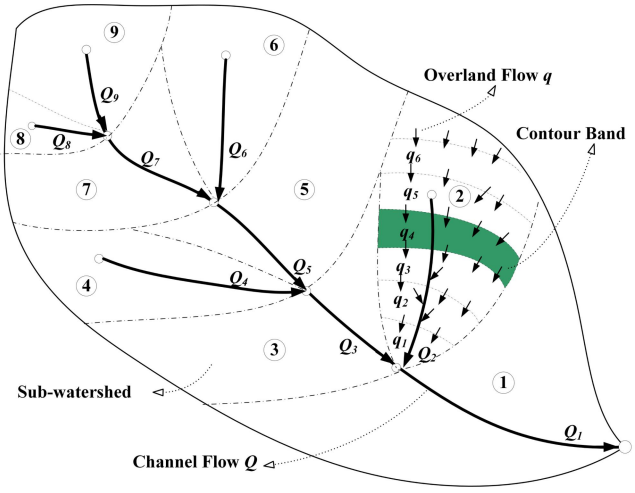

(a)

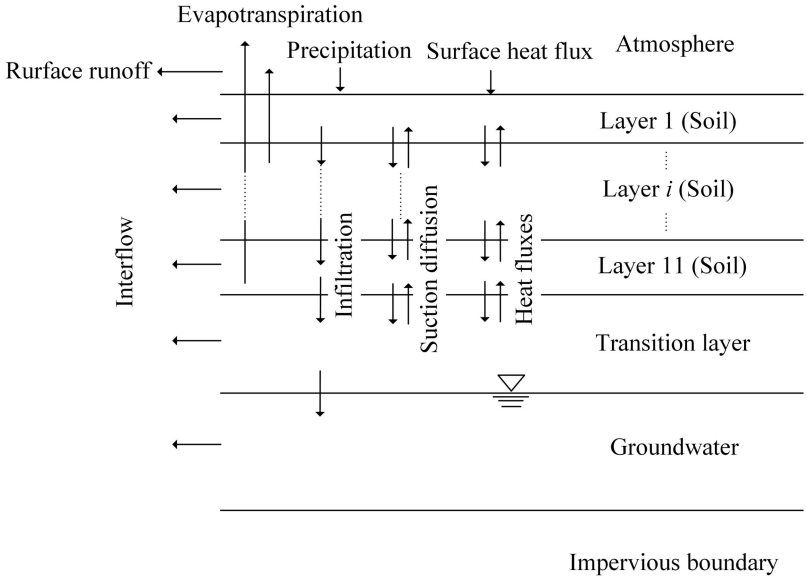

(b)

Figure B1: Horizontal (a) and vertical (b) structure of the WEP-COR model

Water-Heat Transport Simulation

The WEP-COR model divides soil infiltration into two scenarios, heavy rain infiltration and non-heavy rain infiltration, according to the different runoff generation mechanisms. In the non-heavy rain infiltration scenario, the runoff is generated by saturation-excess, the soil vertical water flux transfer can be written as follows (Shang et al., 1997; Wang et al., 2014):

$$\frac{\partial \theta_l}{\partial t} = \frac{\partial}{\partial z}\left[D(\theta_l)\frac{\partial \theta_l}{\partial z} - K(\theta_l)\right] - \frac{\rho_I}{\rho_l}\frac{\partial \theta_I}{\partial t} \quad \text{(B1)}$$

where θ_l is the volumetric content of liquid water in the soil layer (cm^3/cm^3); $D(\theta_l)$ and $K(\theta_l)$ are the unsaturated soil hydraulic diffusivity (cm^2/s) and hydraulic conductivity (cm/s); t and z are the time and space coordinates (positive vertically downward), ρ_l is the water density (kg/m^3).

The Van Genuchten function (Van Genuchten, 1980) was used to describe the upper soil water retention curves:

$$\frac{\theta_l - \theta_r}{\theta_s - \theta_r} = \frac{1}{[1+(\alpha h)^n]^m} \quad \text{(B2)}$$

where θ_s is the saturated water content (cm^3/cm^3); θ_r is the residual water content (cm^3/cm^3); h is the matric suction (cm); α is an empirical parameter (cm^{-1}); n and m are empirical parameters affecting the shape of the retention curve; $m = 1–1/n$.

The hydraulic conductivity was calculated by the Mualem model (Mualem Y, 1986):

$$K(\theta_l) = \begin{cases} K_S & \theta_l = \theta_s \\ K_S\left(\frac{\theta_l - \theta_r}{\theta_s - \theta_r}\right)^{\Omega} & \theta_l \neq \theta_s \end{cases}, \quad \text{(B3)}$$

where $K(\theta_l)$ is the hydraulic conductivity (cm/s) of the soil layer when the liquid water content is θ_l; K_s is the saturated hydraulic conductivity of the soil temperature correction (cm/s); Ω is Mualem's constant.

In the heavy rain infiltration scenario, the runoff is generated by infiltration-excess. The multi-layer unsteady rainfall Green–Ampt model proposed by Jia and Tamai is used (Jia and Tamai, 1998) to calculate the infiltration process. When the infiltration front (INF) reached the m-th layer of soil, the soil infiltration capacity was calculated by the following formulas:

$$f = k_m\left(1 + \frac{A_{m-1}}{B_{m-1}+F}\right) \quad \text{(B4)}$$

$$A_{m-1} = \left(\sum_1^{m-1} L_i - \sum_1^{m-1} \frac{L_i k_m}{k_i} + SW_m\right)\Delta\theta_m \quad \text{(B5)}$$

$$B_{m-1} = \left(\sum_1^{m-1} \frac{L_i k_m}{k_i}\right)\Delta\theta_m - \sum_1^{m-1} L_i \Delta\theta_i \quad \text{(B6)}$$

where f is the infiltration capacity (mm/h); $A_{i\text{-}1}$ is the total water capacity of the soil above the i layer (mm); $B_{i\text{-}1}$ is the error caused by the different soil moisture contents of the soil above the i layer (mm); F is the cumulative infiltration (mm); k_i is the hydraulic conductivity of the i-th soil layer (mm/h); L_i is the soil thickness of the i-th layer (mm); SW_m is the capillary suction pressure at the INF of the m-th layer (mm); $\Delta\theta_i = \theta_s - \theta_l$.

The cumulative infiltration quantity F when the INF reaches the m-th layer is calculated based on whether there is water accumulation on the ground surface. If the ground surface has accumulated water when the INF reaches the m–1th layer, Eq. (B7) was used; otherwise, Eq. (B8) was used:

$$F - F_{m-1} = k_m(t - t_{m-1}) + A_{m-1}\ln\left(\frac{A_{m-1}+B_{m-1}+F}{A_{m-1}+B_{m-1}+F_{m-1}}\right) \quad \text{(B7)}$$

$$F - F_p = k_m(t - t_p) + A_{m-1}\ln\left(\frac{A_{m-1}+B_{m-1}+F}{A_{m-1}+B_{m-1}+F_p}\right) \quad \text{(B8)}$$

$$F_{m-1} = \sum_1^{m-1} L_i \Delta\theta_i \quad \text{(B9)}$$

$$F_p = A_{m-1}\left(\frac{I_p}{k_m} - 1\right) - B_{m-1} \quad \text{(B10)}$$

$$t_p = t_{m-1} + (F_p - F_{n-1})/I_p \quad \text{(B11)}$$

where t is the time; $t_{m\text{-}1}$ is the time when the INF reaches the interface between the m−1 and m layers; t_p is the start time of the water accumulation; F_p is the cumulative infiltration quantity at t_p; I_p is the precipitation intensity at t_p.

The relationship between the water and heat transport of frozen soil is mainly manifested in the dynamic balance of the moisture content of the unfrozen water and the negative temperature of the soil. According to the principle of energy balance, the energy change of each layer in the freeze–thaw system was used for the soil temperature change and water phase change in the system. The heat flux conducted into the soil was calculated using the forced recovery method (Douville et al., 1995; Pitman et al., 1991). The heat flux and temperature of each layer were calculated using the following equation (Chen et al., 2008):

$$H_{i,i+1} = 0.1782\frac{(\lambda_i Z_i + \lambda_{i+1} Z_{i+1})(T_i - T_{i+1})}{(Z_i + Z_{i+1})^2} \text{ and} \quad \text{(B12)}$$

$$T_i = \frac{H_{i-1,i} - H_{i,i+1}}{C_{vi} Z_i}, \quad \text{(B13)}$$

where i is the number of soil layers; $H_{i,i+1}$ represents the sensible heat flux between the i layer and the i+1 layer (MJ/m^2); λ represents the thermal conductivity (W/[m·°C]); Z is the thickness (cm); C_v is the soil volume heat capacity (J/[m^3·°C]); T is the temperature (°C).

Temperature is the driving force of the water phase change. The relationship between the water and heat transport of frozen soil is mainly manifested in the dynamic balance of the moisture content of the unfrozen water and the negative temperature of the soil:

$$\theta_l = \theta_m(T) \quad \text{(B14)}$$

where $\theta_m(T)$ is the maximum unfrozen water moisture content corresponding to a negative soil temperature.

For other details of the WEP-COR model, please refer to Li et al. (2019).